J. Fluid Mech. (1986), *vol.* 170, *pp.* 139–168
Printed in Great Britain

Experimental study of the two-dimensional inverse energy cascade in a square box

By J. SOMMERIA

Gis Madylam, Institut de Mécanique de Grenoble, BP 68, No. 38402,
Saint Martin D'Hères Cedex, France

(Received 3 April 1985 and in revised form 14 February 1986)

A quantitative experimental study of the two-dimensional inverse energy cascade is presented. The flow is electrically driven in a horizontal layer of mercury and three-dimensional perturbations are suppressed by means of a uniform magnetic field, so that the flow can be well approximated by a two-dimensional Navier–Stokes equation with a steady forcing term and a linear friction due to the Hartmann layer. Turbulence is produced by the instability of a periodic square network of 36 electrically driven alternating vortices. The inverse cascade is limited at large scales, either by the linear friction or by the finite size of the domain, depending on the experimental parameters. In the first case, $k^{-\frac{5}{3}}$ spectra are measured and the corresponding two-dimensional Kolmogorov constant is in the range 3–7. In the second case, a condensation of the turbulent energy in the lowest mode, corresponding to a spontaneous mean global rotation, is observed. Such a condensation was predicted by Kraichnan (1967) from statistical thermodynamics arguments, but without the symmetry breaking. Random reversals of the rotation sense, owing to turbulent fluctuations, are more and more sparse as friction is decreased. The lowest mode fluctuations and the small scales are statistically independent.

1. Introduction

Two-dimensional turbulence is relevant in many situations where body forces or boundary conditions prevent the growth of three-dimensional disturbances. This can be observed in rotating flows (Colin de Verdière 1980), in soap films (Couder 1984), or in liquid metals moving under the influence of a strong uniform magnetic field. Generalizations of two-dimensional turbulence known as geostrophic turbulence (reviewed, for example, by Rhines 1979 and McWilliams 1983), provide a first approach to understanding large scale motion of the atmosphere and oceans. While important properties of ordinary turbulent flows, such as the existence of the direct energy cascade, are essentially three-dimensional, an understanding of the large-scale behaviour could be supported by the concepts of two-dimensional turbulence. This point of view was developed by Staquet & Lesieur (1985) for the dynamics of the coherent structures in mixing layers.

A fundamental peculiarity of two-dimensional flows is, in the limit of small viscosities, the vorticity conservation along the fluid particle trajectories, which prevents an energy cascade towards small scales. The existence of an inverse energy cascade towards large scales with a $k^{-\frac{5}{3}}$ energy spectrum and an enstrophy (mean-squared vorticity) cascade towards small scales with a k^{-3} energy spectrum were conjectured by Kraichnan (1967) for a randomly forced turbulence. The enstrophy cascade was also conjectured by Batchelor (1969) for freely decaying

turbulence, but the inverse cascade is then replaced by a growth of the integral scale. These ideas were confirmed in the framework of second-order closures (Kraichnan 1971; Pouquet *et al.* 1975). Review papers were written by Kraichnan & Montgomery (1980) and Lesieur (1983). New developments resulted recently from high-resolution numerical simulations of the two-dimensional Navier–Stokes equations. The problem of the universality of the enstrophy cascade has received much attention. In the calculation of Brachet, Meneguzzi & Sulem (1985), a randomly chosen initial state produces a k^{-3} spectrum after some time. However, other authors, such as McWilliams (1984), observe that the enstrophy transfers can be inhibited by the formation of isolated circular vortices, in a way depending on initial conditions, which leads to spectra steeper than k^{-3}. Numerical investigations of the inverse energy cascade are more difficult, but evidence of a $k^{-\frac{5}{3}}$ inertial range was obtained, and different value of the corresponding two-dimensional Kolmogorov constant are found by different authors (see §6). Beyond the case of homogeneous isotropic turbulence, an interesting question is the nature of the large scales of motion which are created when the inverse cascade reaches the size of a finite domain. This problem arises for example in experiments made in a rotating tank (Hopfinger, Browand & Gagne 1982) where a mean flow is observed, in which it is difficult to know what are the respective influences of angular-momentum transfers owing to three-dimensional motions and of the two-dimensional inverse cascade.

Although important characteristics of two-dimensional turbulence are observed in several of the above-mentioned experimental examples, quantitative comparisons with theory or numerical computations are often difficult. This is due to the unknown effects of some residual three-dimensional perturbations, to uncertainties about the turbulent production, and also to the difficulty of measurements. In order to minimize these drawbacks, we use a thin horizontal layer of mercury subjected to a uniform vertical magnetic field. The suppression of three-dimensional perturbations in such a situation was first observed by a Russian team from Riga (Kit & Tsinober 1971; Kolesnikov & Tsinober 1974; Lielausis 1975), and further theoretical and experimental development was brought out by Sommeria & Moreau (1982), Sommeria (1983), Sukoriansky, Zilberman & Branover (1984) and Selyuto (1984). Turbulence was created in rectangular channels by different kinds of grid and the main properties of the decaying two-dimensional turbulence found by Batchelor (1969) were observed. The turbulent diffusion was very anisotropic, and energy dissipation very weak, while the typical lengthscale was roughly proportional to the time. In addition, k^{-3} energy spectra were clearly measured, but they can also be interpreted by three-dimensional processes (Alemany *et al.* 1979).

In order to obtain simple and well-controlled experimental conditions and to study the inverse energy cascade (from the point of view of Kraichnan 1967), we use electrically driven flows in a closed box. Flow visualizations are made from photographs of the free upper surface, and precise measurements of the local stream function, which is proportional to the electrical potential, are possible. The experimental apparatus, which has already been used by Sommeria & Verron (1984) with a different distribution of the electric currents, is described in §2.1. Electrical measurements can be realized simultaneously at 11 points in order to obtain space structures and spectra directly: the data-analysis methods are given in §2.2. The interpretation of the results is based on a two-dimensional approximation, developed in §3, in which the important non-dimensional number Rh, based upon a typical bottom friction time, is defined. Experimental results concerning the transition to turbulence, the regime of quasi-homogeneous isotropic two-dimensional turbulence,

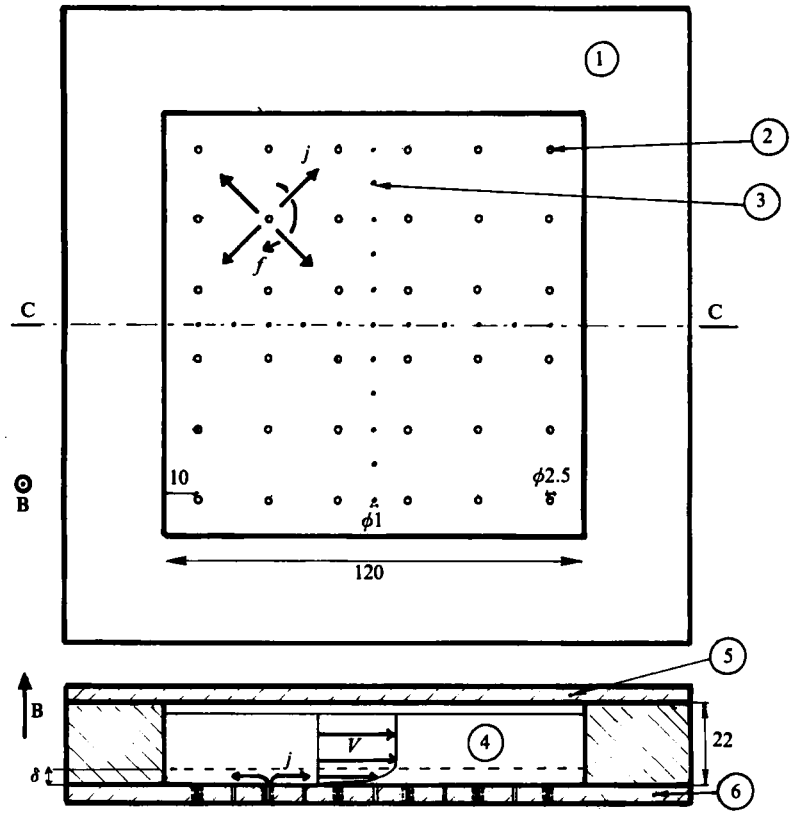

FIGURE 1. The apparatus; the current distribution near one electrode and the velocity profile are schematized. The Hartmann-layer depth is denoted by δ. (1) Copper frame. (2) Electrodes for current injection and electric potential measurements. (3) Electrodes for electric potential measurements only. (4) Mercury. (5) Glass cover. (6) Electrically insulating bottom plate in which electrodes are embedded.

and the regime for which the flow is controlled by the finite size of the domain, are presented in §§4, 6 and 7 respectively. Finally a comparison with some aspects of quasi-geostrophic flows is sketched in §8.

2. The experiments

2.1. *The experimental device*

The experimental apparatus described by Sommeria (1984) is a square box, length $l = 12$ cm, containing a horizontal layer of mercury of thickness a 2 cm (figure 1). It is located in the gap of an electro-magnet producing a uniform vertical magnetic field < 1 Tesla. The upper surface is either free, and in contact with pure nitrogen to avoid oxidation, or rigid, after the formation of a mercury oxide skin. The flow velocity is kept small enough (< 10 cm/s) for free surface waves to be negligible. A periodic square network of 36 alternate sources and sinks of electric current is provided by a corresponding network of electrodes embedded in the bottom of the box. The electric current is provided by a well-regulated d.c. power supply (0–20 A, maximum relative drift 10^{-3}) and equally distributed within a precision of 10^{-3} by 2 sets of 18 equal electric resistances (3 Ω each). Great care is taken to avoid any geometrical or

electrical dissymetry. Since the kinematic viscosity of mercury is 10^{-7} m^2 s^{-1} (ten times smaller than water), the typical Reynolds numbers are fairly high ($> 10^4$), even in a small box.

The investigation of the flow is performed in two ways. The first is to observe the displacement of small floating particles (50–100 μm) following the fluid motion. Of course this method is used only in the free-surface case, although a qualitative observation is still possible from the small vertical deformation of the oxide skin due to pressure differences. The second method is to measure the electric potential on a straight line of 11 electrodes at the middle of the box. Two such perpendicular lines are available (figure 1). The small electric tensions ($\sim$ 1 mV) are amplified 10^3 times, using 11 low-drift operational amplifiers. Digital processing is then performed by a micro-computer with 12-bit resolution.

2.2. *Data analysis*

The instantaneous flow could be measured with fairly good precision (within a few per cent) from photographs, the length of each small trajectory being proportional to the corresponding velocity and to the time of exposure. In practice such visualizations were used only for rather qualitative global observations. Obtaining quantitative statistical information, such as spatial energy spectra, requires high-resolution digital image processing, which was not available.

All the measurements are performed from records of the electric potential. This is a very direct method, its precision being limited only by the electronic noise and thermal drift of the amplifier. A relative precision of 10^{-2} or 10^{-3} can be obtained, especially in a strong magnetic field. The long-time behaviour of the largest scales is investigated from records of the electric potential at the box centre. Time spectra are calculated from these data by fast Fourier transforms. Direct measurements of the spatial structure are obtained from simultaneous records on the line of 11 electrodes. In order to get a smooth profile, the electric potential measured at these 11 points is interpolated on to the line by cubic spline functions. The first space derivative, which is proportional to the transverse velocity component, is calculated analytically from this interpolation. Mean and r.m.s. velocity profiles and spatial autocorrelations are obtained from these results, by averaging over 800 velocity profiles once every 5 seconds. Spatial one-dimensional spectral are calculated either from a direct Fourier transform of the instantaneous potential profile using (A 22) and (A 24), or from the autocorrelation function of the velocity using (25). The correspondence between these two methods is given in the Appendix.

3. The two-dimensional approximation

3.1. *The equations of motion*

Under the effect of a strong uniform vertical magnetic field $\boldsymbol{B}$, the flow can be divided into a two-dimensional core and thin Hartmann boundary layers near the horizontal walls. Their depth δ is constant and is calculated in magnetohydrodynamics textbooks (Shercliff 1965):

$$\delta = \left(\frac{\rho\nu}{\sigma B^2}\right)^{\frac{1}{2}} = \frac{a}{M},$$

where a is the total thickness of the mercury layer, M is the Hartmann number and ρ, ν and σ are respectively the fluid density, viscosity and conductivity. The viscous

friction in the Hartmann layer is transmitted to the whole core by the 'electromagnetic stiffness' along the magnetic-field direction. It corresponds to a force $-\boldsymbol{v}^*/t_{\mathrm{H}}$, where $\boldsymbol{v}^*(x, y, t)$ is the two-dimensional velocity field in the core and $t_{\mathrm{H}} = (a/B)(\rho/\sigma\nu)^{\frac{1}{2}}$, as shown by Sommeria & Moreau (1982). The effect of three-dimensional perturbations is also estimated in that paper, and it should be limited here to small scales without much influence on the dynamics of the energetic scales. Otherwise the Reynolds number calculated from the Hartmann-layer thickness is small enough to be stable and so does not break into a turbulent boundary layer (Sommeria 1986).

The electric currents brought by the electrodes are mainly restricted to the Hartmann layer where they are superimposed on the current associated with the Hartmann friction. However, the driving force is transmitted to the whole core, and the overall force $\bar{\boldsymbol{f}}^*$ on the two-dimensional flow is equal to the integral of $\boldsymbol{j}^* \times \boldsymbol{B}$ along the z-axis. The curl of $\bar{\boldsymbol{f}}^*$ can be expressed from the horizontal divergence of the horizontal $\boldsymbol{j}^*$ component, $\boldsymbol{\nabla}_\perp . \boldsymbol{j}^*$, which is related to the vertical current j_z^* through the bottom boundary by the current conservation,

$$\boldsymbol{\nabla} \times \bar{\boldsymbol{f}}^* = \int_0^a \boldsymbol{\nabla} \times (\boldsymbol{j}^* \times \boldsymbol{B}^*)\, \mathrm{d}z^* = B \int_0^a (\boldsymbol{\nabla}_\perp . \boldsymbol{j}^*)\, \mathrm{d}z^* = B j_z^*/a. \tag{1}$$

So the vorticity production rate is proportional to the injected current density. Some three-dimensional effects are also associated with the current injection. They are localized in an area of width $a/M^{\frac{1}{2}}$, and are investigated by Sommeria (1984, 1986) in simple experimental examples. Due to the corresponding Joule dissipation, the two-dimensional vorticity production should be slightly smaller than (1) in a moderate magnetic field.

Non-dimensional coordinates must be used to compare different experimental results. A natural lengthscale is the box side L, but the velocity scale is not known *a priori*. So we define our non-dimensional time t such that the non-dimensional electric forcing is of order unity. Each real quantity is distinguished from the non-dimensional one by an asterisk.

$$t^* = \left(\frac{\rho a L^2}{BI}\right)^{\frac{1}{2}} t, \quad \boldsymbol{r}^* = L\boldsymbol{r}, \quad \boldsymbol{j}^* = \left(\frac{I}{L^2}\right)\boldsymbol{j}, \tag{2}$$

where I is the total electric current supplied by the d.c. source. The corresponding non-dimensional equation of motion for the velocity field in the two-dimensional core $\boldsymbol{v}(x, y, t)$ is

$$\left.\begin{aligned} \frac{\partial \boldsymbol{v}}{\partial t} + (\boldsymbol{v} . \boldsymbol{\nabla})\, \boldsymbol{v} &= -\boldsymbol{\nabla} P + \frac{\boldsymbol{\nabla}^2 \boldsymbol{v}}{Re} - \frac{\boldsymbol{v}}{Rh} + \boldsymbol{f}(x, y, t), \\ \boldsymbol{\nabla} . \boldsymbol{v} &= 0, \\ \boldsymbol{\nabla} \times \boldsymbol{f} &= j_z(x, y, t), \end{aligned}\right\} \tag{3}$$

$$\left.\begin{aligned} Re &= \left(\frac{L}{\nu}\right)\left(\frac{BI}{\rho a}\right)^{\frac{1}{2}}, \\ Rh &= s\left(\frac{aI}{B\sigma\nu}\right)^{\frac{1}{2}} L^{-1} = s\left(\frac{a}{L}\right)^2 \frac{Re}{M}, \end{aligned}\right\} \tag{4}$$

where s is a constant, equal to 1 when the upper surface is free and equal to $\frac{1}{2}$ when

it is rigid. The electric scheme is such that all the currents that enter the bottom must leave the same way, so that, using (2),

$$\int_0^1 \int_0^1 |j_z(x, y, t)| \, dx \, dy = 2. \tag{5}$$

The validity of the two-dimensional approximation (3) was checked in the same experimental device for particular current distributions. Isolated vortices have been produced by current pulses in Sommeria (1984) and measurements are very close to analytical solutions of (3). A four-vortex steady forcing is used in Sommeria & Verron (1984), and the flow is in good agreement with numerical simulations of (3).

The experimental conditions are determined by the two non-dimensional parameters Re and Rh, which stand for the typical time of lateral viscosity effects and Hartmann friction respectively. The usual Reynolds number Re^* can be known only once velocity is measured:

$$Re^* = \langle v_2^2 \rangle^{\frac{1}{2}} Re,$$

and a typical value of Re^* is 10^4. Otherwise, the parameter Rh is much smaller than Re (between 1 and 40), which means that the Hartmann friction is the main cause of energy dissipation. So one could expect that the results depend mainly on this friction parameter and are almost independent of Re. Conversely, the experimental verification that Rh is the main pertinent parameter is a good test of the validity of the two-dimensional approximation (3).

The stream function ψ and the vorticity ω are important quantities defined as

$$v_x = \frac{\partial \psi}{\partial y},$$

$$v_y = -\frac{\partial \psi}{\partial x},$$

$$\omega = (\nabla \times \boldsymbol{v})_z = -\nabla^2 \psi. \tag{6}$$

An interesting feature of the electrically conducting fluid is that the local stream function can be measured directly. Indeed, the electric currents are confined to the Hartmann layers, so that in the two-dimensional core of the flow, Ohm's law states

$$\nabla \phi^* = \boldsymbol{v}^* \times \boldsymbol{B}. \tag{7}$$

Consequently the electric potential ϕ^*, which can be directly measured, is constant along streamlines and is then proportional to the stream function ψ^*. As a consequence of the impermeability condition, the stream function is constant on the lateral boundary and can be chosen equal to zero without any lost of generality. This condition is in agreement with the constant electric potential at the infinitely conducting walls.

It will be useful to expand the stream function in a Fourier series in order to define spatial spectra. For this purpose one could extend the stream function to a periodic one in x and y with period 1. This extended stream function should be continuous because of the impermeability condition but with its first derivative discontinuous. One can eliminate this drawback by first extending the stream function to a square $[-1, 1] \times [-1, 1]$ by antisymmetry, and then extending it to a periodic one (with period 2). The corresponding Fourier expansion is

$$\psi(x, y) = \sum_{n=1}^{\infty} \sum_{m=1}^{\infty} \hat{\psi}_{nm} \sin n\Pi x \sin m\Pi y, \tag{8}$$

where $$\hat{\psi}_{nm} = 4\int_0^1\int_0^1 \psi(x,y)\sin n\Pi x \sin m\Pi y \,\mathrm{d}x\,\mathrm{d}y,$$

and the vorticity can be expanded by term-by-term differentiations:

$$\omega = -\nabla^2\psi = \sum_{n=1}^{\infty}\sum_{m=1}^{\infty} \Pi^2(n^2+m^2)\,\hat{\psi}_{nm}\sin n\Pi x \sin m\Pi y. \tag{9}$$

This later expansion is convergent everywhere inside the square but not on the boundary itself if $\omega \neq 0$. This discontinuity is associated with an asymptotic behaviour of $\hat{\psi}_{nm}$ as $(n^2+m^2)^{-2}$ for large n and m (see for example Tolstov 1962), which corresponds to a k^{-4} isotropic energy spectrum. This geometrical effect of the boundary could modify the slope of the inertial-range spectrum only if it were steeper than k^{-4}.

3.2. *The energy and enstrophy production*

The total production rates of energy and enstrophy by the force $\boldsymbol{f}$ are written respectively

$$\epsilon(t) = \int\int \boldsymbol{f}_{(x,y)}\cdot\boldsymbol{v}_{(x,y,t)}\,\mathrm{d}x\,\mathrm{d}y = \int\int j_{z(x,y)}\psi_{(x,y,t)}\,\mathrm{d}x\,\mathrm{d}y, \tag{10}$$

$$\eta(t) = \int\int j_{z(x,y)}\omega_{(x,y,t)}\,\mathrm{d}x\,\mathrm{d}y. \tag{11}$$

In the present experiments $j_{z(x,y)}$ can be represented by a network of N^2 alternating positive and negative peaks localized at the electrodes (here $N = 6$). This distribution can be developed in a Fourier series.

$$j_{z(x,y)} = \sum_{n=1}^{\infty}\sum_{m=1}^{\infty} j_{nm}\sin n\pi x \sin m\pi y, \tag{12}$$

where $$J_{nm} = 4\int_0^1\int_0^1 j_{z(x,y)}\sin n\pi x \sin m\pi y\,\mathrm{d}x\,\mathrm{d}y.$$

The current density can be considered to a first approximation as a sum of Dirac functions δ, the Fourier transform of which is (using (5))

$$\begin{aligned} J_{nm} &= 8(-1)^{(n-N)/2N}(-1)^{(m-N)/2N} && \text{if } n \text{ and } m \text{ are even multiples of } N,\\ &= 0 && \text{in the other cases.} \end{aligned} \tag{13}$$

In fact, the electrodes have a finite diameter and some local three-dimensional flows can exist above them, so J_{nm} must decrease as an exponential for large wavenumbers.

The energy and enstrophy production given by (10) and (11) can be expanded in a series made of terms of the type $\hat{\psi}_{nm}J_{nm}$. Since the energy spectrum of two-dimensional turbulence decreases strongly at large wavenumbers (at least in k^{-3}), the first term of the series must be very dominant, especially for the energy production, so that

$$\epsilon_{(x,y,t)} \approx 8\hat{\psi}_{6,6(t)}\sin^2 6\pi x \sin^2 6\pi y \approx \frac{\eta(t)}{72\pi^2}, \tag{14}$$

$$\langle\epsilon\rangle \approx 2\langle\hat{\psi}_{6,6}\rangle \approx \frac{\langle\eta\rangle}{72\pi^2}, \tag{15}$$

where the spatial mean is represented by the angled bracket. More generally the whole dynamics should be well approximated by a steady forcing in the 6, 6 sinusoidal

mode. There is good experimental evidence that, for moderate values of Rh, the flow behaves like a homogeneous isotropic turbulence driven by a random forcing with the two production rates $\langle\epsilon\rangle$ and $\langle\eta\rangle$. The equivalent isotropic forcing should be at a wavenumber close to $6\sqrt{2}$, the modulus of the wave vector (6, 6). In this context, the measurement of $\langle\epsilon\rangle$ and $\langle\eta\rangle$ is an important point. It could be obtained by (15) from a two-dimensional spectral analysis of the velocity field or equivalently from the mean velocity associated with the forcing, which becomes

$$\left.\begin{aligned}\langle v_x\rangle &= 3\pi\langle\epsilon\rangle \sin 6\pi x \cos 6\pi y,\\ \langle v_y\rangle &= -3\pi\langle\epsilon\rangle \cos 6\pi x \sin 6\pi y.\end{aligned}\right\} \tag{16}$$

Alternatively, the rate of energy production can be estimated from an energy balance. Considering that the main dissipation comes from the bottom friction, a simple relation is obtained:

$$\langle\epsilon\rangle = \frac{\langle v^2\rangle}{Rh} = \frac{2\langle v_2^2\rangle}{Rh}. \tag{17}$$

4. The transition to turbulence

The stability properties of the periodic network of alternating vortices are not well understood, although Sivashinski & Yakhot (1985) proposed a mechanism of very large-scale instability. However, the linear bottom friction is not included in their theory, in which the only dissipative effect is the usual viscosity. In the present case the Reynolds number is high and the large scales are strongly damped by the bottom friction, so this theory cannot be used.

The experimental study of the transition is performed in a magnetic field of 1 Tesla with a rigid upper surface. The electric potential at the centre is followed on an oscilloscope, and a visual observation of the flow is also possible from the small deformation of the oxide skin associated with pressure variations. The electric current is slowly increased step by step and a direct transition to a turbulent state occurs at $I = 1.033$ A corresponding to $Rh = 1.78$. This transition is associated with pairings of equal-sign vortices. If we consider that the box is made of 9 smaller boxes each containing 4 vortices, the instability mechanism described in Sommeria & Verron (1984) should occur: two vortices form a bigger one while the others are stretched at the periphery. The perfect-slip boundary conditions used in that paper are compatible with this partition of the box. The corresponding transition threshold for the four vortices is experimentally 1.72 and numerically 1.37, with a spatially sinusoidal steady forcing (Sommeria & Verron 1984). So the idea that the destabilization of the network is associated with the 4-vortex interaction is in good agreement with these results. The difference between the numerical value and the experimental one could be explained by the localization of the vorticity production near the electrodes in the latter.

The complete behaviour near the transition is in fact fairly complex (figure 2). First, when the electric current is decreased once the turbulent state has been reached, the periodic network is obtained again only for $Rh = 1.24$ in the general case. However, in very rare circumstances a steady pattern, represented in figure 3(*a*), can also be reached. Its stability domain extends from $Rh = 1.08$ to 1.55. This flow is the result of the interaction between the 9 vortices at each corner. A similar pattern, represented in figure 3(*b*), can also be obtained, but it is only metastable and goes back to the periodic network after about one minute.

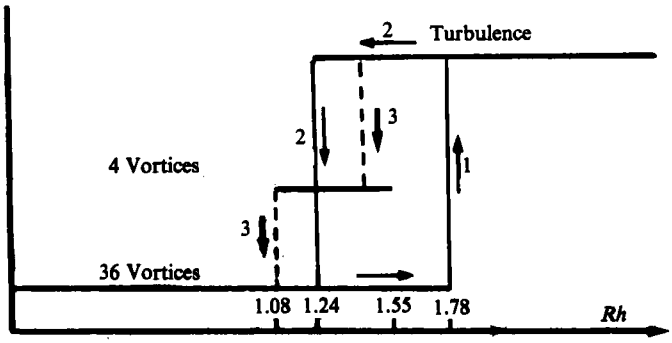

FIGURE 2. Diagram of the transition to turbulence. The three stable regimes are indicated by a full line in their range of stability (the vertical level is arbitrary). When Rh is progressively increased route 1, corresponding to a direct transition to tubulence, is always followed. When Rh is decreased the alternative routes 2 and 3 can be followed.

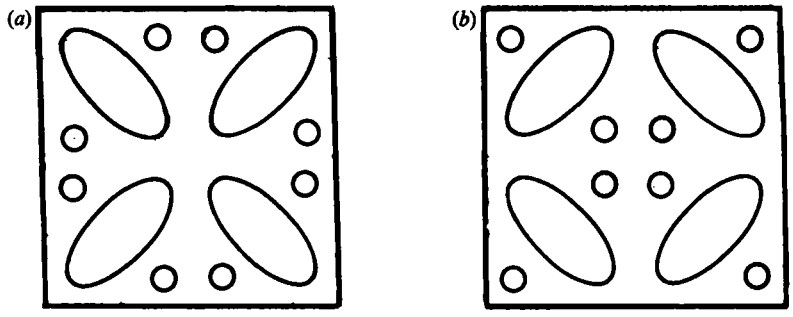

FIGURE 3. Schematic representations of streamlines in the 4-vortex configurations. (*a*) The stable one. (*b*) The metastable one.

5. The turbulent regimes, photographic observations

We are interested in the steady dynamical regimes which correspond to different values of the friction parameter Rh. We also wish to check that the results are not sensitive to the Reynolds number Re, at least when it is large enough. In practice the magnetic field is chosen between 0.125 and 1 Tesla and the total electric current between 0.5 and 16 A. For each run the mercury is initially at rest and the electric current is suddenly switched on. A well-ordered vortex network is then created over a period of a few tens of seconds (figure 4*a*). When $Rh > 1.78$, this network is fully destabilized by pairing processes and a turbulent regime occurs. We then wait about ten minutes in order to get a statistically permanent flow before beginning photography or electric measurements.

The first point apparent in figure 4 (*b–d*) is that the turbulent structures are larger and larger for increasing values of Rh. As the final result of this evolution with Rh, a mean rotating flow is observed (figure 4*d*), in which small vortices are superimposed. The appearance of this mean flow is discussed in §7; however we shall first be concerned with the quasi-homogeneous isotropic regime that occurs for smaller values of Rh.

An easy way to quantify the turbulent scales from photographs like those in figure 4 is to count the mean number $\langle N \rangle$ of vortex cores in the box (figure 5). In practice,

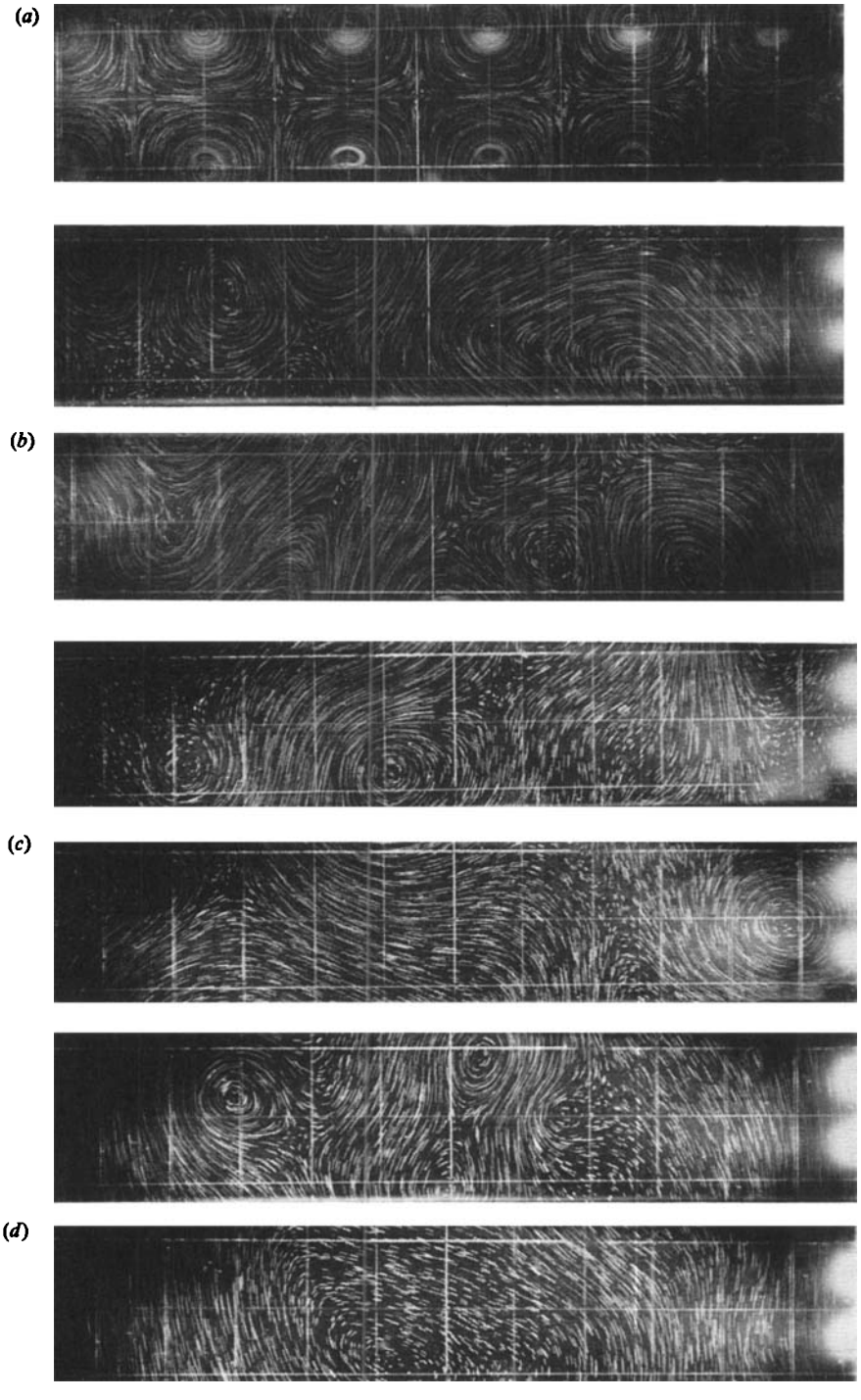

FIGURE 4. Photographs of a central band of the upper surface, using a 45° mirror. The velocity field is represented by the traces of small particles (t is the time of exposure, the scale is 1 cm/division). (*a*) The initial motion when the current is switched on; (*b*) $Rh = 7.27$, $B = 0.48$ Tesla, $t = 195$ ms (2 examples); (*c*) $Rh = 29.1$, $B = 0.24$ Tesla, $t = 114$ ms (2 examples); (*d*) $Rh = 41.1$, $B = 0.12$ Tesla, $t = 195$ ms (2 examples).

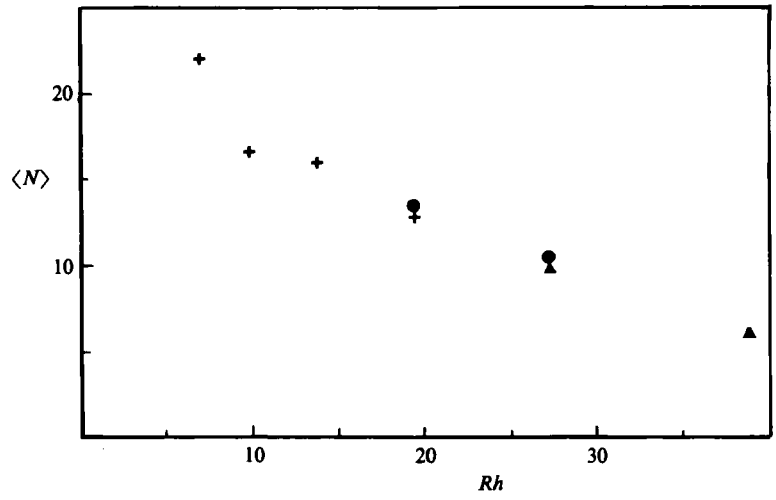

FIGURE 5. Mean number $\langle N \rangle$ of vortex cores in the whole flow versus Rh. +, $B = 0.48$ T; ●, $B = 0.24$ T; ▲, $B = 0.12$ T.

we need to add the results obtained for the different bands of the free surface that can be visualized at any one time. A typical turbulent integral scale can be estimated as $(L^2/\langle N \rangle)^{\frac{1}{2}}$ from a hypothesis of equal-size vortices. In fact this mean number is the result of some small-scale vortices as well as of the large vortices which make the greatest contribution to the turbulent energy. So the integral scale can be underestimated by this method. A better characterization of the inverse cascade is provided by energy spectra and correlation functions. Such calculations are possible from photographs, but they require digital image processing, which has not been undertaken here. These quantities are more easily obtained from electrical measurements which are presented in the next section.

6. The inverse energy cascade of homogeneous isotropic turbulence

6.1. *Mean velocity and r.m.s. fluctuations*

A zero mean value of the velocity is obtained along the line of electric measurements when Rh is smaller than a threshold which will be specified in §6.4. A mean velocity field must exist because of the steady forcing but it vanishes on the measurement line. This mean flow can be calculated from the experimental r.m.s. velocity by (16) and (17). For example for $Rh = 3$ the maximum mean velocity is 0.025. It is definitely smaller than the corresponding r.m.s. of 0.090 (non-dimensional values), and the ratio becomes much smaller for large values of Rh. These results are in agreement with the general impression that the influence of the periodicity is small in the turbulent regime.

The variations of the r.m.s. velocity fluctuations along the line of measurements have a reproducible oscillating structure (figure 6). This structure is very similar for different experimental conditions with a free surface at a given value of Rh. However, the agreement is not so good when we compare these results with those for the rigid surface. In this latter case the amplitude and period of the oscillation are larger. It is not clear whether these differences are due to defects of the two-dimensional approximation or to spurious effects at the boundary with the oxide skin. However,

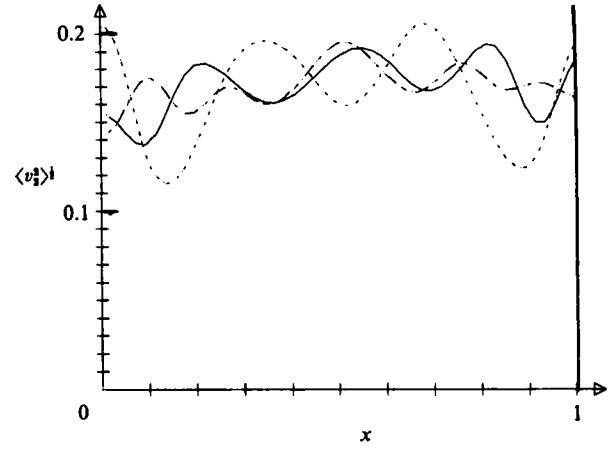

FIGURE 6. The r.m.s. transverse velocity profile along the line of measurements for different experimental conditions corresponding to the same value of $Rh = 10.07$ (non-dimensional position). —, free upper surface, $B = 0.5$ T, $I = 4$ A; —·—·—, free upper surface, $B = 1$ T, $I = 8$ A; ----, rigid upper surface, $B = 0.5$ T, $I = 16$ A.

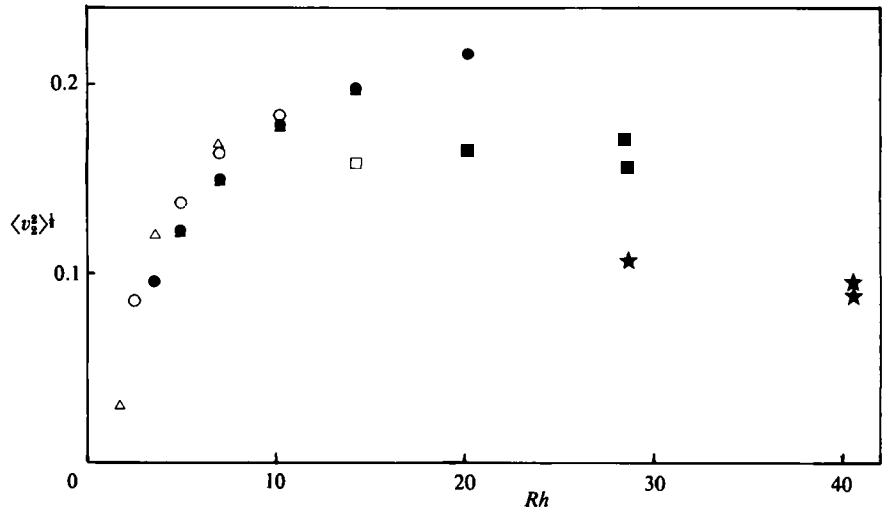

FIGURE 7. R.m.s. transverse velocity $(\langle v_2^2 \rangle)^{\frac{1}{2}}$ averaged on the central third of the box versus Rh. Free surface: ▲, $B = 1$ T; ●, $B = 0.50$ T; ■, $B = 0.25$ T; ★, $B = 0.125$ T. Rigid surface: △, $B = 1$ T; ○, $B = 0.50$ T; □, $B = 0.25$ T.

these oscillations have a fairly small amplitude and the turbulent intensity can be considered as uniform to a first approximation.

Let us define the r.m.s. velocity by averaging over the central third of the box and plot it versus Rh (figure 7). For a fixed magnetic field, this non-dimensional r.m.s. velocity increases with Rh and reaches a constant value at $Rh \approx 20$. The energy production rate $\langle \epsilon \rangle$, given by (17), should then decrease for large values of Rh. Thus the flow is increasingly less correlated to the forcing, and the production mechanism less and less efficient. The non-dimensional results obtained with different experimental conditions are in good agreement for strong magnetic fields. However, the turbulent energy has a tendency to be smaller when the magnetic field is too weak,

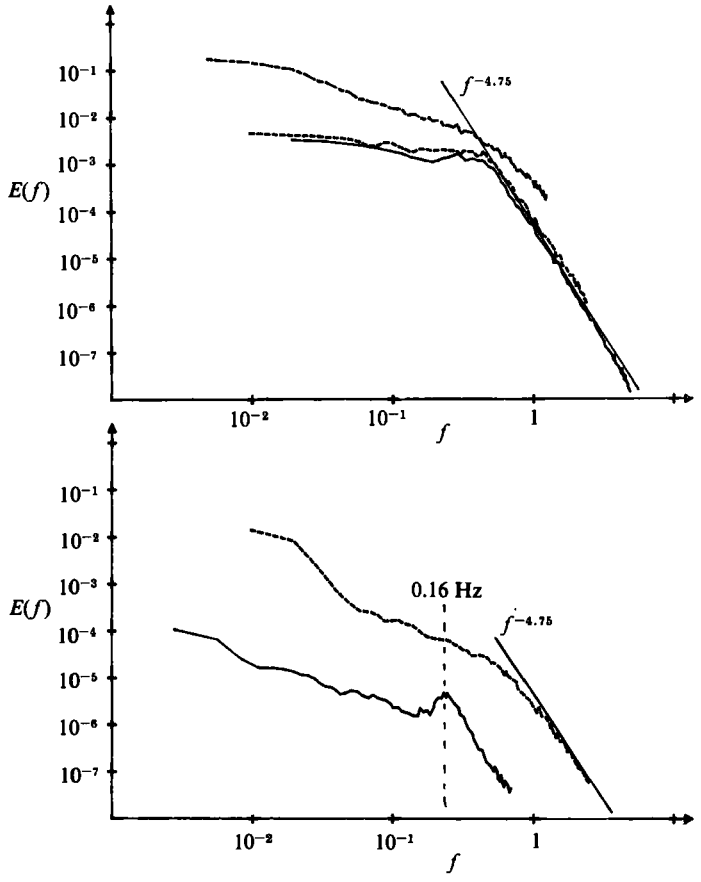

FIGURE 8. Time spectra of the central stream function ψ_1 in log–log coordinates, normalized in such a way that $\int_0^\infty E(f)\,\mathrm{d}f = \langle\psi_1^2\rangle$. The frequency is non-dimensional, the corresponding real frequency in Hz is given by $f^* = \alpha f$, where α is obtained from (2). The upper surface is free except for one case. (*a*) ——, $B = 1$ T, $I = 1$ A ($Rh = 3.56$), $\alpha = 0.50\ \mathrm{s}^{-1}$; ----, rigid surface, $B = 0.5$ T, $I = 2$ A ($Rh = 3.56$), $\alpha = 0.50\ \mathrm{s}^{-1}$; —·—, $B = 1$ T, $I = 16$ A ($Rh = 14.2$), $\alpha = 2.0\ \mathrm{s}^{-1}$. (*b*) ----, $B = 0.25$ T, $I = 16$ A ($Rh = 28.5$), $\alpha = 1.0$; ——, $B = 0.123$ T, $I = 16$ A ($Rh = 40.6$), $\alpha = 1.40\ \mathrm{s}^{-1}$. The mean value $\langle\psi_1\rangle$ is subtracted to ψ_1 before computing the spectrum.

which happens at large Rh for practical reasons. This is because of a loss of energy production due to the three-dimensional effects above the electrodes. The large scale dynamics themselves should be in better agreement with the two-dimensional theory than is indicated by these global results.

6.2. *Time spectra*

Time spectra of the central stream function are obtained from samples of 50000 successive pieces of data. The average is calculated from 210 fast Fourier transforms realized on 512 points. Each sample overlaps the preceding one by 50% and is multiplied by a Blackmann–Harris window.† The spectra are always very smooth, which is proof that the flow is genuinely turbulent as soon as the periodic network

† This window is suitable for investigating steep spectra with minimum perturbations of the sample edges (see Harris 1978).

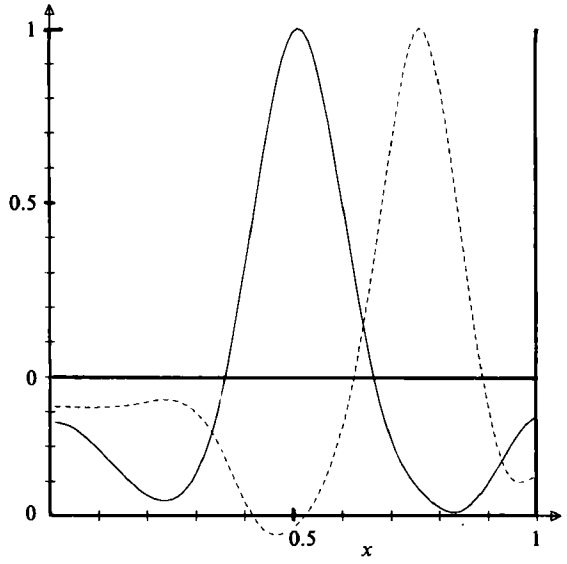

FIGURE 9. Autocorrelation of the transverse velocity component $\langle v_2(x_0)\, v_2(x)\rangle$ along the line of electric measurements. $Rh = 20.1$ ($B = 0.5$ T, $I = 16$ A, free surface), —, $x_0 = 0.5$, ---, $x_0 = 0.75$.

is destabilized. Typical results are plotted in figure 8 with logarithmic coordinates. At large frequencies they exhibit a very steep power law of nearly constant slope of between 4.5 and 4.9. However, it is difficult to distinguish such a steep slope from an exponential curve. For weak values of Rh, the central stream function behaves like white noise for frequencies which are smaller than the inverse of the turnover time; i.e. the correlation time of these large scales is of the order of the turnover time.

The long-time dynamics of the large scales is a random walk under the effect of the eddies corresponding to the injection scale. The large-scale behaviour is quite different for larger values of Rh as is shown in §7. Notice that spectra obtained under very different experimental conditions corresponding to the same value of Rh are in good agreement, which is another validation of the two-dimensional equations (3).

6.3. *One-dimensional spectra*

Some typical autocorrelation functions of the transverse velocity along the line of electrical measurements are represented in figure 9. The similarity of the curves obtained with different origins x_0 for the autocorrelation $\langle v_{2(x_0)}\, v_{2(x_0+x)}\rangle$ is a good indication of the turbulence homogeneity. One-dimensional spectra of the transverse velocity component can be obtained by a Fourier transform of these autocorrelations. This method of calculating spectra is suitable for scales of motion that are definitely smaller than the size of the box, but not for the largest eddies. For example, a global rotation is not taken into account by the correlation function with the origin at the centre, since the corresponding velocity is vanishing there. A more suitable method for this case is to expand the instantaneous velocity profile in Fourier series and to average the square of the coefficients. The relation between these two kinds of one-dimensional spectra is given at the end of the Appendix.

Representative one-dimensional spectra are plotted in figure 10 together with the theoretical slopes $k^{-\frac{5}{3}}$ and k^{-3} and the injection wavenumber estimated in §2. These results are obtained by a Fourier series expansion, so that the wavenumber k is restricted to discrete values ($k = n\pi/L$). Energy is concentrated around the injection

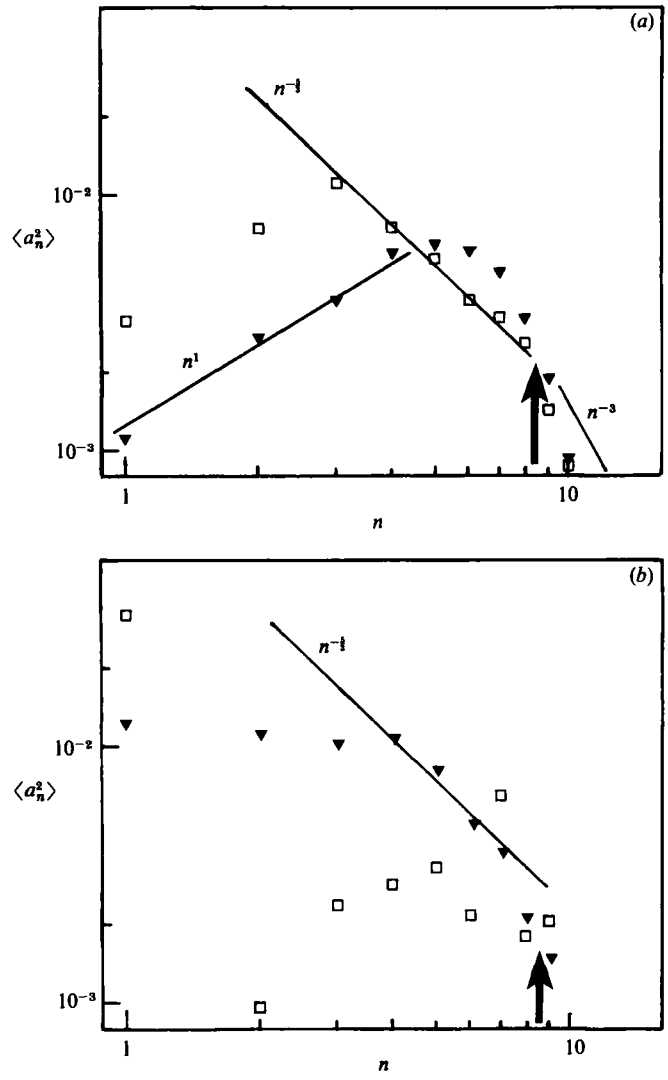

FIGURE 10. One-dimensional spectra of transverse velocity component in log–log coordinates. The points correspond to the 12 first terms of the Fourier series computed from a periodic profile obtained after a symmetrization (see §2.2). The normalization is such that $\sum_1^\infty \langle a_n^2 \rangle = 2\langle v_2^2 \rangle$. The wavenumber is expressed in the unit π/L. The slopes $-\frac{5}{3}$, -3 and 1 are indicated as well as the injection wavenumber. (*a*) ▼, $Rh = 5.04$ (free upper surface, $B = 1$ T, $I = 2$ A); □, $Rh = 14.24$ (rigid upper surface, $B = 0.25$ T, $I = 16$ A); (*b*) ▼, $Rh = 27.4$ (free upper surface, $B = 0.25$ T, $I = 16$ A; □, $Rh = 40.3$ (free upper surface, $B = 0.125$ T, $I = 16$ A.

wavenumber for small values of the friction parameter. For $Rh > 4$, an inverse cascade begins to grow, which is in reasonable agreement with a $k^{-\frac{5}{3}}$ range. However, this process is quickly limited by the size of the domain. Then the $k^{-\frac{5}{3}}$ extends no further, yet the fluctuations of the smallest wavenumber continue to increase progressively until most of the energy is condensed in the largest scale ($n = 1$), corresponding to a global rotation. So the main features observed by flow visualizations are confirmed by these measurements.

The extent of the $k^{-\frac{5}{3}}$ energy spectrum is about half a decade in the best cases,

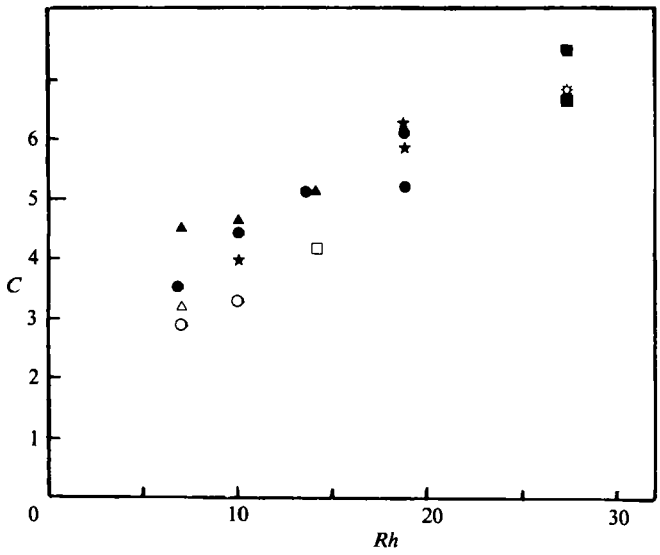

FIGURE 11. Two-dimensional 'Kolmogorov constant' C versus Rh calculated from the spatial spectra. Larger values are an indication of less efficient inverse energy transfers. Free surface: ▲, $B = 1$ T; ●, $B = 0.50$ T; ■, $B = 0.25$ T; ★, $B = 0.150$ T (spectra calculated directly from autocorrelations by (A 8)). Rigid surface: △, $B = 1$ T; ○, $B = 0.50$ T; □, $B = 0.25$ T.

which corresponds to values of Rh roughly between 14 and 30. Below these values, the Hartmann friction drains an important part of the energy along this cascade. Above them, sensible departures from homogeneity and isotropy are due to a global motion at the scale of the box. The two-dimensional Kolmogorov constant can be estimated from these measurements. For this purpose, the first step is to fit the spectrum to a $k^{-\frac{5}{3}}$ law, close to but below the wavenumber of energy injection. To get systematic processing we determine the straight line of slope $-\frac{5}{3}$ (in log–log coordinates) which is the closest to the points corresponding to $n = 4$ to 8. The second step is to relate these one-dimensional spectra to the usual isotropic energy spectra, by using the properties of isotropy and homogeneity. This is done using (A 21) and (A 24), derived in the Appendix. Finally, it is necessary to determine the mean production of energy $\langle \epsilon \rangle$ (dropping the angled brackets for convenience) using relation (17), obtained in §2, by assuming that all the injected energy is dissipated only by Hartmann friction. The two-dimensional Kolmogorov constant C which is determined by this method is roughly independent of the experimental conditions for a given value of the friction parameter Rh (figure 11). This is a good test of the two-dimensional equation (3). The variations of C with Rh are sensible and are between 3 and 7. The inertial range is limited to about half a decade, so it is not surprising that a universal value of C is not reached. For large Rh, the interaction of the largest scales with the boundaries is not negligible, so that the inverse energy transfers should be inhibited, which corresponds to a larger value of C. For small Rh, the existence of an energy sink by Hartman friction at small wavenumbers should enhance the inverse transfers, due to their 'diffusive' properties, i.e. the tendency to smooth the energy spectrum. By this effect, C should be smaller at small Rh than the asymptotic constant. Indeed a value $C = 3$ is obtained by Herring & McWilliams (1985) in a limited inertial range, in the framework of a second-order closure (Test Field Model), while the corresponding asymptotic constant is 6.5 (Kraichnan 1975).

In a larger box, a plateau should exist in the graph of C versus Rh, at between 3 and 7, corresponding to the asymptotic value. This estimation is slightly smaller than the value of 9 obtained by Frisch & Sulem (1984) and is consistent with the value of 5 of Herring & McWilliams. These latter results were obtained by direct numerical simulations (pseudo-spectral scheme) of the two-dimensional Navier–Stokes equation with a random forcing. The value of 14 of Siggia & Aref (1981) calculated by a vortex-in-cell numerical method is much larger.

The other important feature of two-dimensional turbulence is the enstrophy cascade towards small scales. However, the present data do not provide any information about it, since the spatial resolution of the measurements is not good enough: the size of the smallest eddies that can be resolved is about half the injection scale.

Finally, it is worth noting the behaviour of the spectra at small wavenumbers for small values of Rh. Indeed, they are proportional to the wavenumber k to within a good approximation. It is shown in the Appendix that the isotropic energy spectra should behave the same way. Spectra in k^1 correspond to an equipartition of energy in two-dimensional turbulence and should be obtained with a thermodynamic equilibrium between the turbulent modes. However, since the Hartmann dissipation is important in this case and the system should be far from thermodynamic equilibrium, this experimental result is surprising.

7. Interactions of large-scale flows with the boundaries

7.1. *A condensation in the lowest mode*

For $Rh \approx 35$, a global rotation spontaneously appears, superimposed on smaller eddies (visualized in figure 4*d*). Either rotation sense is possible, and random relatively short reversals can occur between these two quasi-stable states, but their probability decreases very quickly with increasing Rh. For $Rh > 41$, the rotation sense can persist for several days and a non-zero large-scale mean flow is measured. The sense can be chosen, then, by means of a convenient initial impulse. The complex structure of this flow is revealed by a mean-velocity profile obtained on the line of electric measurements (figure 12). Velocity reaches a maximum near the walls and some spatial oscillations are superimposed on the large-scale flow; these look analogous to the oscillations of the r.m.s. velocity at smaller values of Rh (figure 6), but are organized in a coherent manner here. Spatial spectra (taking into account both the mean flow and the fluctuations) confirm that most of the energy is condensed in the lowest mode 1, 1 (figure 10*b*). There is also a weaker secondary maximum at the injection wavenumber.

The condensation of most of the energy in the lowest mode was predicted by Kraichnan (1967) by statistical-thermodynamics arguments which we shall briefly summarize. The stream function is expanded by means of a complete orthonormal set of eigenfunctions ψ_n of the Laplacian operator ($\Delta\psi_n = \lambda_n^2 \psi_n$), vanishing on the boundary. This expansion is given by (8) for our square box. If dissipation and forcing are neglected and a maximum cutoff wavenumber is arbitrarily assigned, the system can be considered to be in thermodynamic equilibrium (Kraichnan & Montgomery 1980). Statistical mechanics, taking into account the conservation of both energy and enstrophy, leads to a spectral-energy distribution proportional to $1/(\alpha+\beta\lambda_n^2)$, where α and β are two constants (negative or positive). In the limit $\alpha+\beta\lambda_n^2 \to 0$ the energy of the single lowest mode $n = 1$ becomes much larger than all the others. This behaviour is formally analogous to the Bose–Einstein condensation

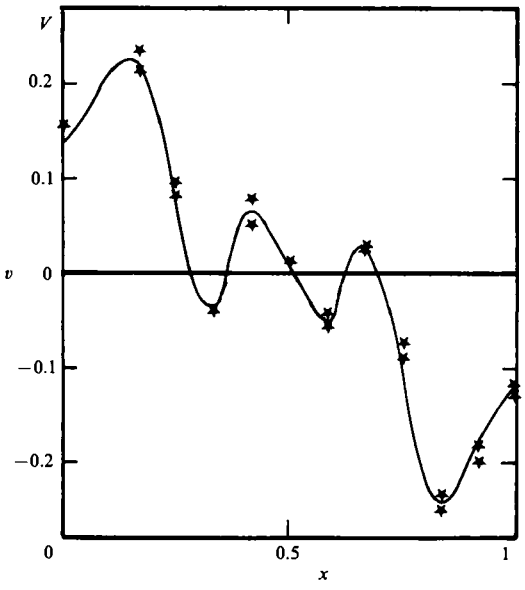

FIGURE 12. Mean transverse velocity profile when no reversal is observed (non-dimensional coordinates). $Rh = 41.1$ ($B = 0.12$ T, $I = 16$ A, free surface).

		1	2	3	4	5	Global
$n = 2$	$10^6 \times \langle a_2^2 \rangle$	27	57	72	50	26	39.5
	ku	3.3	3.2	2.8	3.0	3.1	3.55
$n = 3$	$10^6 \times \langle a_3^2 \rangle$	11.7	25.2	41.0	21.5	10.8	36.8
	ku	3.2	2.8	2.5	2.8	3.0	2.5
$n = 8$	$10^6 \times \langle a_8^2 \rangle$	5.7	5.6	6.0	5.2	5.6	5.6
	ku	2.7	2.8	2.7	2.5	2.7	2.7

TABLE 1. R.m.s. and kurtosis ($\langle a^4 \rangle / \langle a^2 \rangle \langle a^2 \rangle$) of the conditional probability distribution of the three wavenumbers, $n = 2$, 3, 8. These distributions are calculated from samples for which the amplitude of the mode $n = 1$ is in the range labelled by the numbers 1 to 5. These numbers correspond to the ranges $]-\infty, -0.035]$, $[-0.035, -0.015]$, $[-0.015, 0.015]$, $[0.015, 0.035]$, $[0.035, \infty]$ respectively (see also figure 17). The global quantities obtained without any condition on the $n = 1$ mode are indicated in the last column.

in the fundamental state for a perfect quantum gas. One could expect that the artificial cutoff at high wavenumber has then little influence, and that this situation of thermodynamic equilibrium should be approached when the inverse energy cascade is inhibited by the boundary.

Apart from the existence of the condensation phenomenon, the thermodynamic theory cannot be used to interpret several other important experimental features. First, the spatial spectra are not decreasing monotonically for large Rh: there is a secondary maximum near the injection wavenumber (figure 10*b*). However one could consider that only the largest scales are in thermodynamic equilibrium and an enstrophy cascade occurs at small scales. Secondly, the probability distribution of each mode should be Gaussian and it should be decorrelated with the other ones. In fact, the probability distribution of the mode $n = 1$ is split into two main peaks,

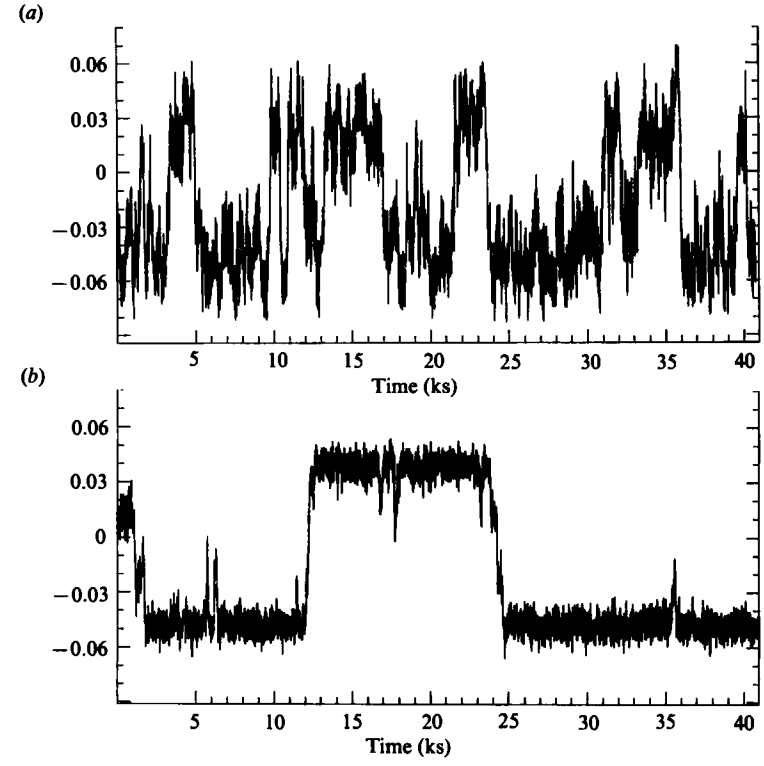

FIGURE 13. Typical time records of the non-dimensional central stream function (free surface, $I = 16$ A). (*a*) $Rh = 36.8$; (*b*) $Rh = 39.5$. Notice the very long timescales.

corresponding to the two senses of rotation (figure 17), and this mode is correlated to its harmonic $n = 3$ (table 1).† A quasi-Gaussian distribution is again obtained at large values of Rh, but around a non-zero mean value. Notice that the Gaussian distribution around 0 is theoretically predicted for a canonical ensemble, i.e. a system in statistical equilibrium with a large 'thermal bath', for which energy fluctuations can be important. Since the energy fluctuations of our system are limited, the microcanonical ensemble, which describes an isolated system, should be more appropriate. It would be interesting to develop such a theory to ascertain whether the existence of the mean rotation can be explained only by thermodynamic arguments.

A remark should be made about the generality of these results for different boundary shapes. In a square box, the condensation in the mode $n = 1$ is not forbidden by the conservation of angular momentum. Indeed, the electric forcing is symmetric and cannot bring any rotation sense by itself, but the momentum of the pressure forces at the lateral walls can balance the decay due to the bottom friction. In a circular box, the pressure forces are radial and have no momentum, so the total angular momentum must vanish in the limit of large Reynolds numbers. The condensation in the single lowest mode is then forbidden. It should occur in the two vortex modes (calculated with Bessel functions). Since two such modes (corresponding

† In fact, we measure one-dimensional modes which correspond to a superposition of several two-dimensional modes, but the qualitative behaviour should be the same.

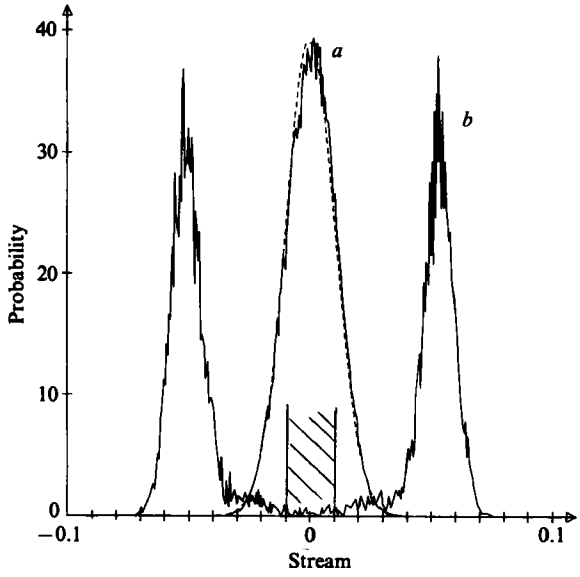

FIGURE 14. Probability density of the central non-dimensional stream function (in abscissa). (*a*) $Rh = 3.56$ (free surface $B = 1$ T, $I = 1$ A); the distribution is very close to Gaussian (represented by a dashed line). (*b*) $Rh = 40.3$ (free surface, $B = 0.125$ T, $I = 16$ A); two symmetric peaks are obtained, corresponding to the two senses of rotation. The probability is integrated in the hatched area to plot one point of figure 15.

to the x- and y-directions exist, important fluctuations of a mode amplitude can occur without dramatic fluctuations of the total energy. So their probability distribution can be close to Gaussian without symmetry breaking. The same remark applies to period boundary conditions, for which the lowest mode is also degenerate, due to the phase indetermination.

7.2. *The transition between the quasi-isotropic turbulence and the mean flow*

An easy way to quantify the rotation rate is to measure the stream function at the centre (i.e. the electric potential). For moderate values of Rh this quantity has a Gaussian probability distribution (figure 14*a*) around 0, and the time spectra are flat for frequencies lower than the inverse of a typical turnover time (figure 8). These two features are a characteristic of a random walk due to the effect of small eddies. As Rh is increased, the probability distribution is first flattened and then split into two peaks corresponding to the two rotation senses (figure 14*b*) and the importance of very small frequencies increases (figure 8).

For $Rh > 35$, one can distinguish phases of constant rotation sense followed by relatively short changes of sense (figure 13). Some isolated 'events' can also disturb the global flow without changing its sense. The typical duration between reversals increases very rapidly with the friction parameter, and it is tempting to look for a transition threshold. For this purpose, increasing values of Rh are obtained with decreasing magnetic fields for a constant electric current of 16 A. For $Rh = 41$, no reversals were observed during two 100-hour records, one for each sense (chosen by means of a suitable initial condition). So we can consider that a non-zero mean flow is obtained from a practical point of view. However, a plot of the mean frequency of the reversals versus Rh, using a logarithmic vertical scale, suggests that it decreases roughly exponentially without any well-defined threshold (figure 15). It is

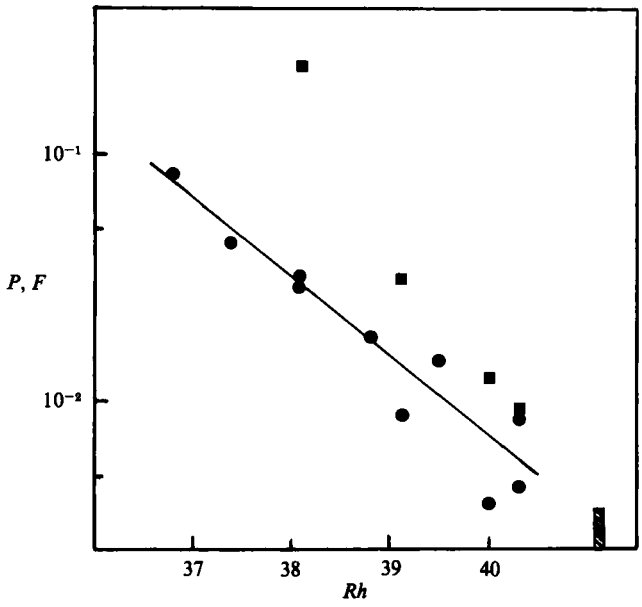

FIGURE 15. Behaviour near the transition between the quasi-isotropic regime and the mean flow. Two characteristic quantities are plotted versus Rh (semi-logarithmic coordinates). ■, The mean frequency of reversals in units per 10^4 s. (The hatched area at $Rh = 41.1$ is an estimation of the reversal frequency based upon the fact that no reversal is observed during 100 hours.) ●, Probability of finding the central stream function between ± 0.01 (integral of the probability density in the hatched area of figure 14).

of course more and more difficult to avoid statistical fluctuations of this frequency as Rh is increased. Since many 'events' bring a zero central stream function but do not lead to a reversal, the transition can be more easily characterized by the value of the probability distribution of the central stream function near 0. These results reported in figure 15 are also in agreement with exponential behavour without a well-defined threshold.

If Rh is increased above 41, fluctuations of the central stream function have again a quasi-Gaussian distribution but around the mean value, and the time spectra get flatter and flatter at small frequencies (figure 8*b*). There is also a broad spectral peak, corresponding to a period of rotation. Otherwise the fluctuation amplitude continues to decrease.

7.3. *Interactions between the different spatial modes*

The reversals correspond to an important variation of the total angular momentum of the fluid and therefore cannot be directly due to small external perturbations. The change of rotation sense occurs during a few minutes, which is short compared with the long timescales but still longer than the turnover time. We did not notice any well-defined mechanism for the reversals. Otherwise, the duration of two successive stages of constant rotation sense is not clearly related. So it seems that the reversals are due to an exceptional fluctuation of the large-scale flows under the random effect of small eddies.

Simultaneous records of the amplitude of the different spatial wavenumbers during reversals bring some insight to this problem. Such records are obtained by a Fourier transform of the electric potential at the 11 measurement points, and a typical

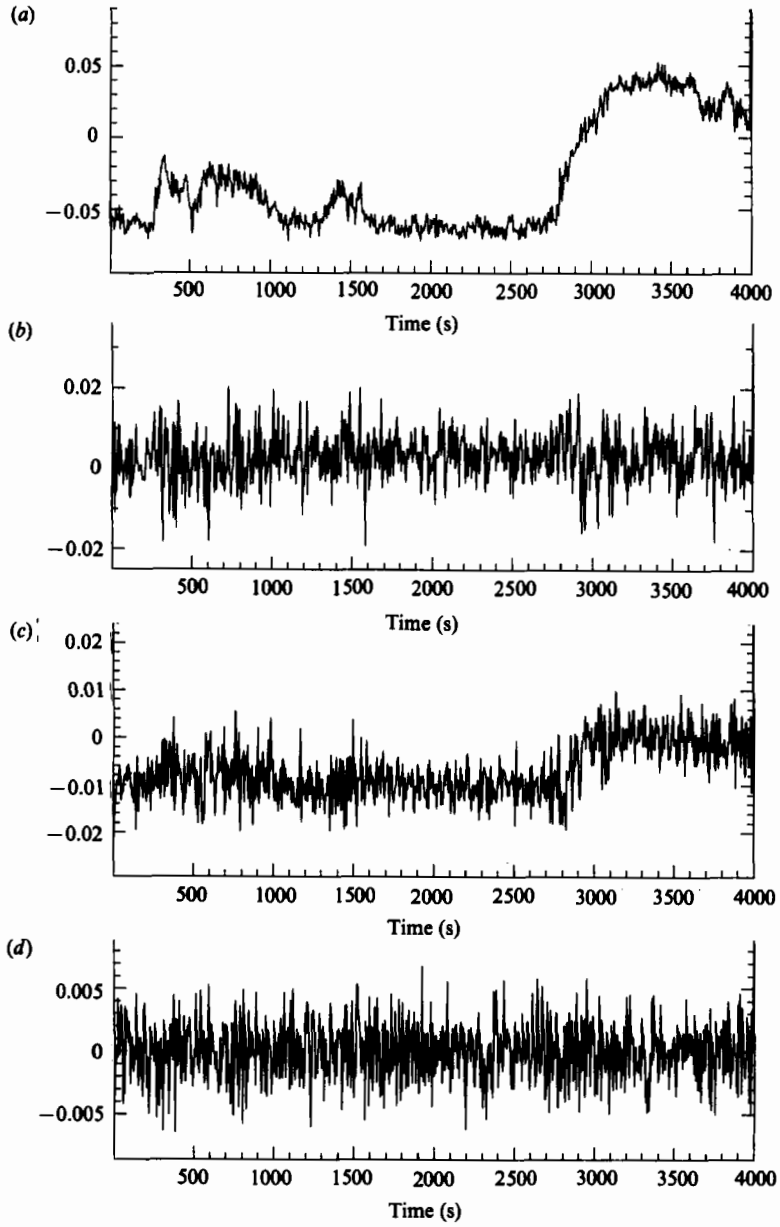

FIGURE 16. Simultaneous records of the time evolution of the non-dimensional amplitude of different wavenumbers (free surface, $I = 16$ A, $B = 0.132$ T; $Rh = 39.2$). (*a*) $n = 1$, (*b*) $n = 2$, (*c*) $n = 3$, (*d*) $= 8$. The evolution of $n = 1$ is very well correlated to the central stream function.

sample is shown for $n = 1$, 2, 3 and 8 in figure 16. The mode $n = 1$ is dominant and is well correlated with the stream function at the centre. The mode $n = 3$ is a harmonic of $n = 1$ with the same symmetry and it is not surprising that they are correlated. The modes $n = 2$ and $n = 8$ seem to be uninfluenced by the reversals. These qualitative observations can be made more precise by the determination of the probability distribution of these modes (figure 17). First of all, a complex structure

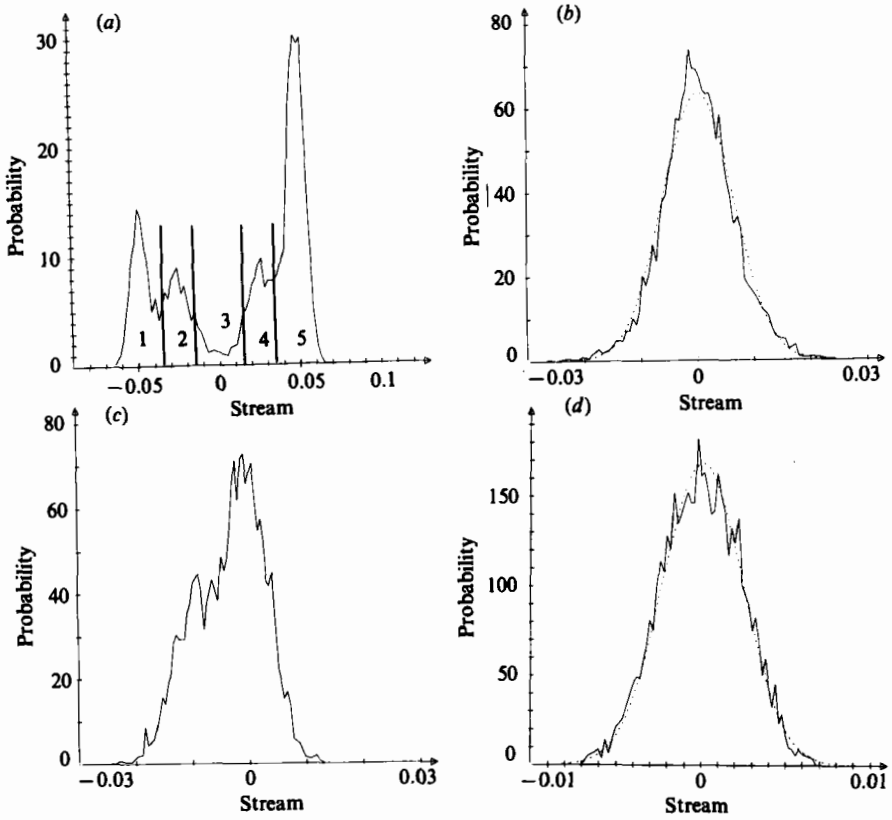

FIGURE 17. Probability distribution of the wavenumbers. (*a*) $n = 1$, (*b*) $n = 2$, (*c*) $n = 3$, (*d*) $n = 8$. The ranges 1, 2, 3, 4, 5 in (*a*) are used to calculate the conditional probabilities of table 1.

for $n = 1$ is revealed. The two main peaks are related to the two senses of rotation. Their height is not equal, probably due to a small experimental dissymmetry. Beside them, two secondary peaks are observed which correspond to the relative stability of an intermediate state that can be observed during reversals (figures 13 and 16*a*). The distribution for small-scale flows ($n = 8$) is very close to a Gaussian with a kurtosis† of 2.8, so that they seem to be insensitive to the large-scale-flow behaviour. The kurtosis of $n = 2$, equal to 3.5, is an indication that the corresponding dynamics is more complicated. More precise information can be obtained by calculating the joint probability distribution for $n = 1$, $n = 2$ and $n = 1$, $n = 8$. To avoid excessive statistical fluctuations a partition into 5 sets for the $n = 1$ amplitude is used (represented in figure 17), and the results obtained from a total set of 6000 samples are summarized in table 1. The fluctuations of the mode $n = 2$ are more important when the rotation associated with $n = 1$ is smaller. So this mode is involved in the reversal process. The small scales represented by $n = 8$ are independent of the global rotating flow. In other words, the occurrence of the reversals is not associated with a strong fluctuation of the energy production.

† The kurtosis of the random variable a is defined as $\langle a^4\rangle/\langle a^2\rangle\langle a^2\rangle$ and is equal to 3 for a Gaussian.

8. Similarities with geophysical flows

Two-dimensional equations similar to (3) are generally used to model large-scale atmospheric motions in the quasi-geostrophic approximations. The transfer of barotropic energy from the scale L_I of production by the baroclinic instability to larger eddies and to the mean zonal flow is generally assimilated by a two-dimensional inverse energy cascade. This latter is limited at a scale L_β (Rhines 1979) by the variation of the horizontal component of the Coriolis force with latitude (β-effect). There is also a limitation due to the surface friction in the planetary boundary layer.

This drag is usually modelled by a linear term $-v/t_E$ identical with the Hartmann friction. The coefficient $1/t_E$ can be estimated from the measured depth of the planetary boundary layer by taking into account the Ekman effect. The production mechanism by the baroclinic instability involves thermal phenomena and is much more complicated than the steady force of the present experiments. This latter is exactly analogous to the vorticity production by sources and sinks in the bottom of the rotating tank as used by Colin de Verdière (1980). In such experiments, a β-effect can be obtained by means of large-scale topography. A similar method cannot be used in an MHD device: energy would be dissipated rather than propagated as Rossby waves. However, the limitation of the inverse energy cascade by the β-effect is roughly similar to the confinement between two parallel walls, east–west oriented a distance L_β apart. There is no limitation in the perpendicular direction (Rhines 1979), so a better analogy would be provided by an experiment in a large-aspect-ratio rectangular box.

In spite of many shortcomings it is useful to compare the experimental parameters and the atmospheric ones which are typically

$$L_I \approx 1000 \text{ km},$$
$$L_\beta \approx 3000 \text{ km},$$
$$t_E \approx 10^6 \text{ s},$$
$$\epsilon \approx 3 \times 10^{-4} \text{ m}^2 \text{ s}^{-3}.$$

The non-dimensional qualities which must be used in (3) can be obtained from the non-dimensional length l and time t

$$l = l^*/L_\beta,$$
$$t = (t^*/T_E)\, Rh.$$

The experimental parameter Rh is such that the corresponding non-dimensional forcing is of the order of unity. However, the ratio between the injection scale L_I and the largest available one L_β is half the experimental one, so that the comparison should be made on the injection of energy ϵ, which is independent of the scale to a first approximation,

$$Rh^3\epsilon = \epsilon L_\beta^{-2} t_E^3 \approx 30.$$

The value is obtained experimentally for $Rh \approx 20$, ϵ being calculated from the turbulent energy by (17). It corresponds to a regime for which the limitation of the inverse energy cascade is mainly due to friction effects, but for which a global rotation with random reversals begins to appear. There could be some analogies between this global rotation and persistent atmospheric anomalies such as blocking (M. Lesieur, private communication). By proceeding with this comparison one should expect that such anomalies are more persistent in atmospheric situations for which the product $\epsilon L_\beta^{-2} t_E^3$ is especially large.

9. Conclusions

The previous investigations of quasi-two-dimensional turbulence in liquid metals submitted to a uniform magnetic field, made in channels, have been concerned with decaying turbulence. Here, we are able to investigate the inverse energy cascade of a statistically steady turbulence, by means of a well-controlled electric forcing. A two-dimensional dynamics is well achieved for $B \gtrsim 0.25$ Tesla, probably because of the relatively small depth and the 'soft' forcing mechanism. This affirmation is supported by the good correspondence of the non-dimensional results obtained with the same value of Rh for different experimental conditions (free and rigid upper surface, different magnetic fields). Direct agreement with solutions of the two-dimensional Navier–Stokes equation was also obtained in very similar situations by Sommeria & Verron (1984) and Sommeria (1984). Measurements of the small three-dimensional perturbations, for example by the potential difference between top and bottom, should also be interesting. Notice however that a test of the two-dimensional dynamics by this method is difficult. Indeed, in a strong magnetic field, turbulence can be kinematically two-dimensional, i.e. with a very anisotropic structure, but still much influenced by Joule dissipation (Alemany *et al.* 1979).

The results can be divided into three parts.

(i) An instability of a square, periodic network of alternating vortices by pairing processes is clearly identified. This result is a demonstration that two-dimensional turbulence can be generated by a hydrodynamic instability without any random forcing.

(ii) The first experimental measurement of the two-dimensional $k^{-\frac{5}{3}}$ inverse energy cascade is obtained. These experiments are made in a fairly strong magnetic field, and the non-dimensional results depend mainly on Rh (figures 7 and 11), which is a good proof of the two-dimensional dynamics. There is no doubt about the sense of the energy transfers since the forcing scale is clearly known. More direct measurements of the rate of energy transfer could be provided by bispectra (third-order moments). The turbulence spatial homogeneity is not good (figure 6) and the influence of the forcing anisotropy is unknown, although its square symmetry is not apparent on visualizations. However, the consistency of the two-dimensional Kolmogorov constant with recent numerical simulations made with a random forcing is encouraging. Further experiments should be performed in a larger box, which is not a major technical problem, in order to be closer to an asymptotic inertial range. The spatial spectra were measured directly and accurately by means of the line of electrodes. However, the spatial resolution was not good enough to investigate the enstrophy cascade.

(iii) When friction is small enough, most of the energy is condensed in the lowest mode, which can be interpreted by statistical-thermodynamics arguments. However, the corresponding appearance of a mean flow is not predicted in the framework of canonical ensembles. It would be interesting to know whether it can be explained by a more suitable statistical-thermodynamics theory or whether a specific dynamical theory is needed. Notice that the appearance of a mean flow is related to the existence of a single lowest mode, and should not exist when the lowest mode is degenerate, as in a circular box or with periodic boundary conditions. Indeed, a long-time numerical study of the two-dimensional inverse energy cascade limited by the periodic boundary conditions was performed by Hossain, Matthaeus & Montgomery (1983). In that work, about 90 % of the turbulent energy is eventually concentrated in the lowest mode, but no mean flow is obtained.

This condensation corresponds to a fairly sharp transition with the parameter Rh, but a well-defined threshold is not observed. The typical time between two successive reversals increases very rapidly with Rh, and becomes several orders of magnitude greater than the turnover time. Because of this timescale separation and the spectral separation between the lowest mode and the injection one, a statistical theory could probably provide interesting results. The study of this long-time behaviour, which is presently very costly by numerical computations, could provide some new ideas about quasi-two-dimensional geophysical flows. Indeed, in the atmosphere a maximum scale L_β is imposed by the β-effect, in a similar way to that in a closed domain. Otherwise, there are striking analogies between the reversals of the rotation sense and the reversals of the Earth's magnetic field. Other experimental systems, as in Creveling *et al.* (1975), and models with few degrees of freedom, as the Lorenz system, can display such behaviour. However, the present mechanisms, associated with inverse energy transfers at high Reynolds number, could be more relevant for geophysical flows.

For practical reasons, the large values of Rh were obtained with a moderate magnetic field, and we have doubts about the two-dimensional dynamics. The existence of the global rotation was checked with a 36-vortex forcing in a numerical simulation of (3) by Sommeria & Verron (1985). A comparison of the long-term behaviour was not undertaken because of the computation cost. So, although the largest scales are clearly two-dimensional for geometrical reasons, one can wonder about the influence of small-scale three-dimensional perturbations on the turbulent fluctuations. Incidentally, it would be interesting to study the cases for which the small-scale perturbations are fully three-dimensional, in a very weak magnetic field or with other kinds of forcing.

Useful discussions with U. Frisch, M. Lesieur, R. Moreau and J. Verron are gratefully acknowledged. Pertinent modifications were also suggested by O. Lielausis and J. McWilliams, as referees. Thanks are due to R. Bolcato for the realization of the experimental facility and to A. Tupin for the typing of the manuscript.

Appendix. Different definitions of the energy spectrum in two-dimensional homogeneous isotropic turbulence

Relations between the different definitions of the energy spectrum and the autocorrelation functions for three-dimensional homogeneous isotropic turbulence are given in textbooks (e.g. Hinze 1975, p. 205). Some results concerning two-dimensional turbulence were published by Hutchings (1955), Lilly (1973) and Mory (1984). However, some additional results are needed in order to calculate the two-dimensional Kolmogorov constant from the measurements.

The isotropic energy spectrum $E(k)$ is usually defined from the Fourier transform $\phi_{ij}(\boldsymbol{k})$ of the autocorrelation tensor $R_{ij}(\boldsymbol{r})$ by the following relations (δ is the space dimension):

$$R_{ij}(\boldsymbol{r}) = \langle U_i(\boldsymbol{x})\, U_j(\boldsymbol{x}+\boldsymbol{r})\rangle, \tag{A 1}$$

$$\phi_{ij}(\boldsymbol{k}) = \frac{1}{(2\pi)^\delta} \int R_{ij}(\boldsymbol{r})\, \mathrm{e}^{-\mathrm{i}\boldsymbol{k}\cdot\boldsymbol{r}}\, \mathrm{d}^\delta \boldsymbol{r}, \tag{A 2}$$

$$E(k) = 2\pi k^2 \phi_{ii}(k) \quad \text{(three-dimensional)}, \tag{A 3}$$

$$E(k) = \pi k\, \phi_{ii}(k) \quad \text{(two-dimensional)}. \tag{A 4}$$

Velocity measurements are limited to a straight line, so that longitudinal spectra $E_1(k)$ and transverse ones $E_2(k)$ are naturally obtained from the corresponding correlation functions $f(r)$ and $g(r)$.

$$f(r) = \langle v_1(x)\, v_1(x+r)\rangle, \tag{A 5}$$

$$g(r) = \langle v_2(x)\, v_2(x+r)\rangle, \tag{A 6}$$

$$E_1(k) = \frac{1}{2\pi}\int_{-\infty}^{+\infty} f(r)\, \mathrm{e}^{-\mathrm{i}kr}\, \mathrm{d}r, \tag{A 7}$$

$$E_2(k) = \frac{1}{2\pi}\int_{-\infty}^{+\infty} g(r)\, \mathrm{e}^{-\mathrm{i}kr}\, \mathrm{d}r. \tag{A 8}$$

As a consequence of incompressibility these two correlation functions are related

$$g(r) = \frac{\mathrm{d}(rf)}{\mathrm{d}r}, \tag{A 9}$$

and the corresponding relation between E_1 and E_2 can be obtained by a Fourier transform of each term of (A 9).

$$E_2(k) = -k\frac{\mathrm{d}E_1}{\mathrm{d}k}. \tag{A 10}$$

It is now useful to get the isotropic correlations and spectra from the corresponding one-dimensional quantities. As a direct consequence of isotropy,

$$R_{ij}(r) = \frac{f(r)-g(r)}{r^2} r_i r_j + g(r)\,\delta_{ij}, \quad R_{ii}(r) = f(r)+g(r). \tag{A 11}$$

A relation between $E(k)$ and $R_{ii}(r)$ can be obtained by integrating in spherical shells in definition (A 2),

$$E(k) = \frac{2}{\pi}\int_0^{\infty} kr \sin kr\, R(r)\, \mathrm{d}r \quad \text{(three-dimensional)}, \tag{A 12}$$

$$E(k) = \frac{1}{2}\int_0^{\infty} kr\, J_0(r)\, R(r)\, \mathrm{d}r \quad \text{(two-dimensional)}, \tag{A 13}$$

where J_0 is the zeroth-order Bessel function. By comparing (A 12) with a suitable combination of (A 7) and (A 8), a differential equation for $E_1(k)$ can be obtained. The solution of this equation leads to (Hinze 1975, p. 209)

$$E_1(k) = \frac{1}{2}\int_k^{\infty} \mathrm{d}p \frac{E(p)}{p}\left(1-\frac{k^2}{p^2}\right) \quad \text{(three-dimensional)}, \tag{A 14}$$

$$E_2(k) = \frac{1}{4}\int_k^{\infty} \mathrm{d}p \frac{E(p)}{p}\left(1+\frac{k^2}{p^2}\right) \quad \text{(three-dimensional)}. \tag{A 15}$$

(The one-dimensional spectra defined here are equal to half the spectra of Hinze.) A similar relation for two-dimensional turbulence is less easy to obtain because of the Bessel function in (A 13). A useful intermediate step is to write the sum E_1+E_2 in the following form, using (A 7), (A 8) and (A 11):

$$E_1(k)+E_2(k) = \int_{-\infty}^{+\infty} \phi_{ii}(\boldsymbol{k}+\boldsymbol{l})\, \mathrm{d}l, \quad \boldsymbol{k}.\boldsymbol{l} = 0. \tag{A 16}$$

Then, $E_1(k)+E_2(k)$ can be related to the isotropic spectrum by a simple change of variable

$$E_1(k)+E_2(k)=\frac{2}{\pi}\int_k^\infty \frac{E(p)}{(p^2-k^2)^{\frac{1}{2}}}\,\mathrm{d}p. \tag{A 17}$$

This relation was given in another context by Babiano, Basdevant & Sadourny (1985). By means of (A 10), a differential equation for E_1 is obtained, and its resolution leads to

$$E_1(k)=\frac{2}{\pi}\int_k^\infty \frac{(p^2-k^2)^{\frac{1}{2}}}{p^2}E(p)\,\mathrm{d}p \quad \text{(two-dimensional)}, \tag{A 18}$$

$$E_2(k)=\frac{2}{\pi}\int_k^\infty \frac{k^2}{p^2(p^2-k^2)^{\frac{1}{2}}}E(p)\,\mathrm{d}p \quad \text{(two-dimensional)}. \tag{A 19}$$

A.1. *Behaviour of one-dimensional spectra in the inertial range*

If the isotropic energy spectrum is equal to $C\epsilon^{\frac{2}{3}}k^{-\frac{5}{3}}$ above a wavenumber k_c, the one-dimensional spectra $E_1(k)$ and $E_2(k)$ have the same behaviour with the respective coefficients C_1 and C_2. Relations (A 18) and (A 19) lead to

$$C_1=\frac{3}{8}\left(\frac{2C}{\pi}\right)\int_0^\infty (ch\theta)^{-\frac{5}{3}}\,\mathrm{d}\theta \approx 0.267\,C, \tag{A 20}$$

$$C_2=\frac{5}{8}\left(\frac{2C}{\pi}\right)\int_0^\infty (ch\theta)^{-\frac{5}{3}}\,\mathrm{d}\theta \approx 0.446\,C. \tag{A 21}$$

A.2. *Behaviour of the one-dimensional spectra for small wavenumbers*

Let us suppose that the isotropic spectrum is equivalent to k^n, $n>0$ as $k\to 0$. Then the longitudinal spectrum $E_1(k)$, calculated by (A 18), behaves as a constant

$$E_1(k)\sim\frac{2}{\pi}\int_0^\infty \frac{E(p)}{p}\,\mathrm{d}p \quad \text{as } k\to 0.$$

So $E_1(k)$ is not suitable for an experimental determination of the behaviour of the isotropic spectrum at small wavenumbers.

The behaviour of the transverse spectrum can be obtained by supposing that the isotropic spectrum is equal to αk^{-n} for $0<k<k_c$, where k_c is a fixed cutoff. The integral of (A 19) can be split into two terms by integrating from k to k_c and then from k_c to ∞. The first term can be rearranged by assuming $k \ll k_0$, and we get

$$E_2(k)=\frac{2}{\pi}\left[\alpha k^n\int_0^\infty (ch\theta)^{n-2}\,\mathrm{d}\theta+k^2\int_{k_c}^\infty \frac{E(p)\,\mathrm{d}p}{p^2(p^2-k^2)^{\frac{1}{2}}}\right].$$

If $n<2$, the first term is the dominant one as $k\to 0$, and $E_2(k)$ behaves in the same way as the isotropic spectrum. If $n>2$, the second term is dominant and

$$E_2(k)=\left(\frac{2}{\pi}\int_0^\infty \frac{E(p)}{p^3}\,\mathrm{d}p\right)k^2,$$

so that the slope of the one-dimensional spectrum is independent of the behaviour of the isotropic spectrum at small wavenumbers.

A.3. *Calculation of the energy spectrum in a square box*

Concepts of homogeneous isotropic turbulence can be used in a square box for scales which are sufficiently small. One-dimensional energy spectra can be obtained from

velocity measurements along the median straight line (described in §2) in two different ways. The first one is to calculate the transverse correlation function $g(r)$ by (A 6), and its Fourier transform (A 5) does not depend on the origin x for a really homogeneous turbulence. In the present case, taking the origin at the box centre is the most natural choice. The second method is to extend the instantaneous velocity profile to a periodic one with a symmetry as is done in §3. It is then possible to expand it in Fourier series

$$v_2(x) = \sum_{n=1}^{\infty} a_n \cos n\pi x, \tag{A 22}$$

$$a_n = 2\int_0^1 v_2(x)\cos n\pi x\,\mathrm{d}x = -2n\pi\int_0^1 \psi(x)\sin n\pi x\,\mathrm{d}x,$$

and to consider $\langle a_n^2\rangle$ as a one-dimensional energy spectrum. These two definitions are equivalent in the limit of a large box. Indeed $\langle a_n^2\rangle$ can be written as a double integral which can be split into two terms.

$$\langle a_n^2\rangle = 2\int_0^1 \mathrm{d}x_0 \int_{-1}^1 \mathrm{d}r\,\langle v_2(x_0)\,v_2(x_0+r)\rangle\cos n\pi r$$

$$+2\int_0^1 \mathrm{d}x_0 \int_{-1}^1 \mathrm{d}r\,\langle v_2(x_0)\,v_2(x_0+r)\rangle\cos n\pi(2x_0+r), \tag{A 23}$$

if we increase the size of the box enough, we need only consider the large values of n, so that the second term vanishes, and the first one can be rearranged by using homogeneity and the definition of $g(r)$,

$$\langle a_n^2\rangle = 4\pi E_2(n\pi) \quad \text{for } n\to\infty. \tag{A 24}$$

REFERENCES

ALEMANY, A., MOREAU, R., SULEM, P. L. & FRISCH, U. 1979 Influence of an external magnetic field on homogeneous turbulence. *J. Méc.* **18** (2), 277.

BABIANO, A., BASDEVANT, C. & SADOURNY, R. 1985 Structure functions and dispersion laws in two-dimensional turbulence. *J. Atmos. Sci.* **42** (9), 941.

BATCHELOR, G. K. 1969 Computation of the energy spectrum in homogeneous two-dimensional turbulence. *Phys. Fluids. Suppl.* **2** (12), 233.

BRACHET, M. E., MENEGUZZI, M. & SULEM, P. L. 1985 Numerical simulation of decaying two-dimensional turbulence. In *Macroscopic Modelling of Turbulent Flows*. Lecture Notes in Physics, vol. 230, p. 347. Springer.

COLIN DE VERDIÈRE, A. 1980 Quasi geostrophic turbulence in a rotating homogeneous fluid. *Geophys. Astrophys. Fluid Dyn.* **15**, 213.

COUDER, Y. 1984 Two-dimensional turbulence in a laboratory experiment. *J. Phys. Lett.* **45**, 353.

CREVELING, H. F., DE PAS, J. F., BALADI, J. Y. & SCHOENHALS, R. J. 1975 Stability characteristics of a singlephase free convection loop. *J. Fluid Mech.* **67**, 65.

FRISCH, U. & SULEM, P. L. 1984 Numerical simulation of the inverse cascade in two-dimensional turbulence. *Phys. Fluids* **27** (8), 1921. Erratum: *Phys. Fluids* 1985, **28**, 438.

HARRIS, F. J. 1978 On the use of windows for harmonic analysis with the discrete Fourier transform. *Proc. IEEE* **66** (1), 51.

HERRING, J. H. & MCWILLIAMS, J. C. 1985 Comparison of direct numerical simulation of two-dimensional turbulence with two-point closure: the effect of intermittency. *J. Fluid Mech.* **153**, 229.

HINZE, J. O. 1975 *Turbulence*. McGraw-Hill.

HOPFINGER, E. J., BROWAND, F. K. & GAGNE, Y. 1982 Turbulence and waves in a rotating tank. *J. Fluid Mech.* **125**, 505.

HOSSAIN, M., MATTHAEUS, W.H. & MONTGOMERY, D. 1983 Long time states of inverse cascades in the presence of a maximum length scale. *J. Plasma Phys.* **30** (3), 479.

HUTCHINGS, J. W. 1955 Turbulence theory applied to large scale atmospheric phenomena. *J. Met.* **12**, 263.

KIT, L. G. & TSINOBER, A. B. 1971 Possibility of creating and investigating two-dimensional turbulence in a strong magnetic field. *Magnitnaya Gidrodinamika* **3**, 27.

KOLESNIKOV, Y. B. & TSINOBER, A. B. 1974 Experimental investigation of two-dimensional turbulence behind a grid. *Isv. Akad. Nauk. SSSR Mech. Zhid. i Gaza* **4**, 146.

KRAICHNAN, R. H. 1967 Inertial ranges in two-dimensional turbulence. *Phys. Fluids* **10**, 1417.

KRAICHNAN, R. H. 1971 An almost-markovian Galilean-invariant turbulence model. *J. Fluid Mech.* **47**, 513.

KRAICHNAN, R. H. 1975 Statistical dynamics of two-dimensional flow. *J. Fluid Mech.* **67**, 155.

KRAICHNAN, R. H. & MONTGOMERY, D. 1980 Two-dimensional turbulence. *Rep. Prog. Phys.* **43**, 549.

LESIEUR, M. 1983 Introduction à la turbulence bidimensionnelle. *J. Méc.* (Special issue on Two-dimensional turbulence), p. 5.

LIELAUSIS, O. 1975 Liquid metal magnetohydrodynamics. *Atomic Energy Rev.* **13** (3), 527.

LILLY, D. K. 1973 Lectures in sub-synoptic scales of motions and two-dimensional turbulence. In *Dynamic Meteorology* (ed. P. Morel), p. 353. Reidel.

MCWILLIAMS, J. C. 1983 On the relevance of two-dimensional turbulence to geophysical motions. *J. Méc.* (Special issue), p. 83.

MCWILLIAMS, J. C. 1984 The emergence of isolated, coherent vortices in turbulent flow. *J. Fluid Mech.* **146**, 21.

MORY, M. 1984 Turbulence dans un fluide soumis à forte rotation. Thesis at the University of Grenoble (France).

POUQUET, A., LESIEUR, M., ANDRE, J. C. & BASDEVANT, C. 1975 Evolution of high Reynolds number two-dimensional turbulence. *J. Fluid Mech.* **72** (2), 305.

RHINES, P. B. 1979 Geostrophic turbulence. *Ann. Rev. Fluid Mech.* **11**, 401.

SHERCLIFF, J. A. 1965 *A Textbook of Magnetohydrodynamics.* Pergamon.

SELYUTO, S. F. 1984 Effect of magnetic field on formation of turbulent structure behind arrays of different configurations. *Magnitnaya Gidrodinamika* **3**, 55.

SIGGIA, E. D. & AREF, H. 1981 Point vortex simulation of the inverse cascade in two-dimensional turbulence. *Phys. Fluids* **24** (1), 171.

SIVASHINSKI, G. & YAKHOT, V. 1985 Negative viscosity effects in large-scale flows. *Phys. Fluids* **28** (4), 1040.

SOMMERIA, J. 1983 Two-dimensional behaviour of MHD fully developed turbulence ($Rm \ll 1$). *J. Méc.* (Special issue), p. 169.

SOMMERIA, J. 1984 Two-dimensional behaviour of electrically driven flows at high Hartmann numbers, 4th Beer Sheva Seminar on MHD flows and turbulence, Israel. *Proceedings in AIAA Progress in Aeronautics and Astronautics.*

SOMMERIA, J. 1986 Electrically driven vortices in a strong magnetic field. *J. Fluid Mech.* (submitted).

SOMMERIA, J. & MOREAU, R. 1982 Why, how and when MHD turbulence becomes two-dimensional. *J. Fluid Mech.* **118**, 507.

SOMMERIA, J. & VERRON, J. 1984 An investigation of non linear interactions in a two-dimensional recirculating flow. *Phys. Fluids* **27** (8), 1918.

SOMMERIA, J. & VERRON, J. 1985 The two-dimensional inverse energy cascade in a confined domain: numerical and laboratory experiments. *5th Turbulent Shear Flow Symp.* Cornell University, Ithaca.

STAQUET, C. & LESIEUR, M. 1985 Study of the mixing layer from the point of view of two-dimensional turbulence. *5th Turbulent Shear Flow Symp.* Cornell University, Ithaca.

SUKORIANSKY, S., ZILBERMAN, L. & BRANOVER, H. 1984 Experiments in duct flows with reversed turbulent energy cascades. 4th Beer Sheva Seminar on MHD flows and turbulence, Israel. *Proceedings in AIAA Progress in Aeronautics and Astronautics.*

TOLSTOV, C. P. 1962 *Fourier Series.* (Series in applied maths, trans. from Russian.) Prentice-Hall.